Optogenetic inhibition quenches the integration of sensory input in the cortex

Ambrosone Manuel [a,b,c], Montagni Elena [a,b], Resta Francesco [a,c,d], Curti Lorenzo[e], Mannaioni Guido[e], Masi Alessio[e], Pavone Francesco Saverio[a,c,d], Allegra Mascaro Anna Letizia[a,b*]

[a] *European Laboratory for Non-Linear Spectroscopy, Florence, Italy.*

[b] *Neuroscience Institute, National Research Council, Pisa, Italy.*

[c] *Physics and Astronomy Department, University of Florence, Sesto Fiorentino, Italy.*

[d] *National Institute of Optics, National Research Council, Sesto Fiorentino, Italy.*

[e] *Department of Neurosciences, Psychology, Drug Research and Child Health, University of Florence, Florence, Italy.*

ABSTRACT

Significance: Many fundamental processes of brain computation, such as sensory perception and motor control, heavily rely on the mesoscopic dynamics of activity across the cerebral cortex. Manipulating mesoscale activity and observing its effects across multiple brain regions is crucial for understanding the causal link between cortical dynamics and behavior.

Objective: The goal of this study was to develop a novel all-optical system that allows inhibition of excitatory neurons while simultaneously monitoring cortical responses at arbitrary sites across the entire dorsal cortex of mice.

Methods: We combined wide-field imaging and optogenetics to create a mesoscale all-optical approach, enabling simultaneous monitoring and manipulation of cortical activity using light. Intravenous injection of two PHP.eB AAVs enabled the whole-brain co-expression of the red-shifted calcium indicator jRCaMP1b and the inhibitory actuator stGtACR2, with stable expression over several weeks. This system was calibrated, and the effects of inhibition on sensory responses were tested.

Results: Increasing laser power progressively reduced spontaneous activity at the site of irradiation. A single 5-second pulse on the barrel field cortex significantly decreased the amplitude of sensory-evoked responses, not only in the stimulated region but across the entire stimulated hemisphere.

Conclusions: This novel all-optical system enables targeted inhibition while concurrently monitoring mesoscale cortical activity. It provides insights into the dynamics of cortical circuits and offers a milestone for investigating the causal links between neuronal activity and behavior. Future research can use this tool to address sensory responsiveness impairments in neurological and neuropsychiatric disorders.

Keywords: Optogenetics, all-optical, whiskers stimulation, inhibition, stGtACR2, barrel field cortex

*Corresponding author. Via Giuseppe Moruzzi,1 - 56124 – Pisa, Italy. Neuroscience Institute, National Research Council.

E-mail: allegra@lens.unifi.it (Allegra Mascaro Anna Letizia)

1. Introduction

Establishing a causal link between neural activity patterns across the entire brain and behavior is a major challenge in contemporary neuroscience. In the last decades, optical tools were increasingly adopted for disentangling this connection[1]. In the context of light-mediated control of neuronal activity, optogenetics demonstrated reversible depolarization or hyperpolarization of neurons through the illumination of light-gated ion channels with specific wavelengths[2]. Optogenetic tools, taking advantage of genetically encoded actuators for the activation or inhibition of neurons, hold significant promise for neuromodulation studies[3][4]. Recently, these tools have enabled precise neuromodulation by providing targeted inhibition of neuronal activity, allowing controlled perturbation of cortical responses to peripheral stimuli during active sensing at single cell resolution[5]. In this study, the authors leveraged the newly developed GtACR2, an anion-conducting channelrhodopsin from the cryptophyte *Guillardia theta* optimized for the in vivo silencing of neuronal activity with blue light (480 nm)[6][7][8]. Compared to other inhibitory actuators, GtACR2 shows positive photon-ion stoichiometry and good single-channel conductance[9]. Because of its improved light sensitivity, low axonal excitation, and high photocurrent, the soma-targeted variant (stGtACR2) is more effective for targeted silencing[9]. Due to its minimal responsivity above 560 nm wavelengths, it can be used in

combination with red-shifted genetically encoded indicators, like RCaMPs, for simultaneous inhibition and imaging of cortical activity. RCaMP sensors are well-suited for tracking changes in calcium concentration, a direct parameter of neuronal activity[1][10]. They also provide several benefits when compared to the GCaMP family, including reduced photodamage, minimal hemodynamic interference, and increased maximal imaging depth[11][12]. Large-scale wide-field fluorescence imaging (WFFI) of red-shifted indicators is now commonly used for the measurement of cortex-wide neuronal activity[13][14][15][16]. By combining WFFI with optogenetic tools, it is now possible to measure and modulate large neuronal populations simultaneously using only light. Recently, this combination has been leveraged to perform large-scale all-optical monitoring and excitation of cortical activity[17][18][19][20][21]. Albeit stGtACR2 has been used in combination with red-shifted indicators to investigate small neuronal circuits[22], the consequences of local optogenetic inhibition on the cortical dynamics at the mesoscopic scale are largely unexplored. By leveraging WFFI in combination with the red-shifted calcium indicator jRCaMP1b and the blue-light actuator stGtACR2, we established a robust framework for investigating the large-scale effects of targeted cortical inhibition. Importantly, we validated the efficacy of our tool in reducing the cortical response to peripheral whiskers' stimulation across the entire stimulated hemisphere.

2. Material and methods

A total of 7 female littermates C57BL/6 mice were used. All experiments were performed in accordance with the guidelines of the Italian Minister of Health (aut. n. 721/2020). All animals were housed in standard condition cages with a 12h light/dark cycle and food and water ad libitum. The experimental group included 4 mice while 3 mice were used as sham.

2.1. Virus injection

In order to induce the transfection of the excitatory neurons with the fluorescent calcium indicator jRCaMP1b and the optogenetic actuator stGtACR2, 4 mice were injected with a single retro-orbital injection of two different AAV-PHP.eB mixed. The final injected solution was prepared diluting in 112,5 µL of saline solution, 25 µL of indicator (ssAAV-PHP.eB/2-mCaMKIIα-NES_jRCaMP1b-WPRE-hGHp(A), 1.2x10E13 vg/ml) and 12,5 µL of actuator (ssAAV-PHP.eB/2-mCaMKIIα-stGtACR2_mCerulean-WPRE-bGHp(A), 1.7x10E13 vg/ml) obtained from the Viral Vector Facility, Zurich. The sham group of animals (n =3 mice) were injected with a solution of 25 µL of indicator and 112,5 µL of saline.

2.2. Intact skull window surgery

This procedure was performed as described by Montagni and colleagues[23]. Briefly, 10 days post injection (dpi) mice were anesthetized with isoflurane (3% for induction, 1–2% for maintenance) and positioned in a stereotaxic apparatus (KOPF, model 1900). Ophthalmic gel (Lacrilube) was applied to protect their eyes, and body temperature was maintained using a warming pad. After administering local lidocaine, the skin and periosteum were removed and reference points were marked (bregma and lambda). A custom-made head bar was attached and secured with dental cement (Super Bond C&B – Sun Medical) posterior to lambda. Following surgery, mice were allowed to recover in a controlled environment with food and water available.

2.3. In vivo imaging setup and procedures

2.3.1. Widefield fluorescence microscope

Imaging and optogenetic stimulation are performed with a custom-made wide-field setup based on our previous works[19][21]. Shortly, the jRCaMP1b excitation source was a red LED (595nm LED light, M595L3 Thorlabs, New Jersey, United State) with a bandpass filter (578/21 nm, Semrock, Rochester, New York, USA) and a dichroic mirror (606nm, Semrock, Rochester, New York, USA) directing light through an objective (TL2X-SAP 2X Super Apochromatic Microscope Objective, 0.1NA, 56.3 mm WD, Thorlabs) towards the skull. The stGtACR2 actuator was stimulated with a continuous wave laser (lambda = 473 nm, OBIS 473 nm LX 75mW, Coherent, Santa Clara, CA, USA) merged into the imaging path via a dichroic beam splitter (FF484-Fdi01-25 336, Semrock, Rochester, New York, NY, USA). The system used a random-access scanning head with two acousto-optic deflectors (DTSXY400, AA Opto-Electronic, Orsay France) and a laser beam with an approximate size of 200 µm. Fluorescence emitted by jRCaMP1b was captured through a bandpass filter (630/69, Semrock, Rochester, New York, USA) and imaged onto

a high-speed CMOS camera (Orca Flash 4.0 Hamamatsu Photonics, NJ, USA) at 40 Hz with 512x512 pixels resolution that provided a 11.6x11.6 mm² field-of-view of the mouse cortex.

2.3.2. Wide-field imaging in awake mice

Head-fixed imaging sessions were performed 20 and 30 dpi. Considering the bregma and lambda position, mice were centered to cover the entire field of view (FOV). Image stacks from each session were registered using a custom-made software. Optogenetic calibration was performed on the first imaging session (20 dpi), while in the second imaging session (30 dpi), whiskers stimulation was performed. LED light intensity was 4mW.

2.3.3. Calibration of optogenetic irradiation

Laser stimulation patterns were generated using two orthogonally-mounted Acousto-optic Deflectors (AA Opto-electonic). A reference image of the FOV was used to target the laser beam on a selected cortex area (x=32.8mm on the right and y=10.3mm behind the bregma; barrel-field cortex: BFD). Single-pulse laser irradiation consisted of one pulse (10 ms ON) repeated for 10 times (15 s pre-stim, 11 s post-stim each session) at increasing laser powers (0.15 – 0.32 – 0.82 –1.66 – 3.34 – 6.85 – 10.4 mW). 5-second laser irradiation consisted of 5 seconds of irradiation repeated for 10 times (15 s pre-stim, 6 s post-stim each session) at different laser power (0.15 – 0.32 – 0.82 mW).

2.3.4. Whiskers stimulation

Single air puffs (60 ms long) were presented to the left whiskers 40 times before and after ten times 5-s laser irradiation at 0.82 mW. Imaging session consisted of 15 s pre-stim, 11 s post-stim. The whiskers are stimulated using the Picospritzer III from General ValveTM. The tube was positioned approximately 2 centimeters away from the whiskers.

2.4. Electrophysiology and confocal imaging

2.4.1. In vivo spike recording

Forty days after injection (40dpi), electrophysiological signals were recorded in the BFD cortex of 2 mice using a Parylene C-insulated tungsten microelectrode (A-M Systems) with an impedance of 2 MΩ. The electrode was advanced through a small hole in the skull into layer 5 of the BFD cortex (800 µm below the dura) using a motorized micromanipulator (EXFO Burleigh PCS6000). Signals were amplified with a 3000 AC/DC differential amplifier, sampled at 10 kHz, high-pass filtered at 0.1 Hz, and low-pass filtered at 10 kHz. A reference electrode was placed on the motor cortex. Spikes were extracted by high-pass filtering the local field potential (LFP) at 1000 Hz, isolating fast (~<2 ms), biphasic potential transients.

2.4.2. Ex vivo electrophysiology

From 1 mouse, brain slices (350 µm) containing the BFD were obtained using a vibroslicer (Leica VT1000S) in ice-cold carboxygenated cutting solution (Sucrose 206mM, Glucose 25mM, NaHCO3 25mM, KCl 2.5mM, NaH2PO4 1.25mM, MgSO4 3mM, CaCl2 1mM). After at least 1 hour in warm artificial cerebrospinal fluid (NaCl 130mM, KCl 3.5mM, NaH2PO4 1.25mM, NaHCO3 25mM, Glucose 10mM, CaCl2 1mM, MgSO4 2mM, 32-34 °C), slices were placed in a recording chamber under a Nikon Eclipse E600FN microscope. Electrophysiological recordings used borosilicate capillaries (Harvard Apparatus) filled with K+ gluconate solution (120mM K-Gluconate, 15mM KCl, 10mM HEPES, 1mM EGTA, 2mM MgCl2, 5mM Na2Phosphocreatine, 0.3mM Na2GTP, 4mM MgATP, pH 7.3), resulting in 3–4 MΩ resistance. Signals were sampled at 10 kHz and filtered at 2 kHz with an Axon Multiclamp 700B. The stGtACR2 silencing effect was assessed using whole-cell current clamp configuration, applying 100 pA depolarizing steps and 3 seconds of 470 nm LED stimulation to activate the inhibitory channel.

2.4.3. Ex vivo confocal imaging

Mice were perfused with 20–30 mL of 0.1 M PBS (pH 7.6) and 100 mL of 4% paraformaldehyde (PFA). Brain coronal slices (100 mm thick) were cut with a vibrating-blade microtome (Vibratome Series 1500—Tissue Sectioning System). Considering the BFD position, imaging was performed with a Nikon Eclipse TE300C2 laser confocal scanning microscope (Nikon) equipped with a Nikon Plan Apo 20x air objective. The setup was equipped with 408 nm and 561 nm lasers to simultaneously excite jRCaMP1b and stGtACR2 respectively. Emission filters were 472/10 nm and 630/69 nm.

2.5. Data analysis

All data analyses were performed in MATLAB (MathWorks), ImageJ (Fiji), and Origin.

2.5.1. Quantification of in vivo cortical expression of jRCaMP1b and stGtACR2

To evaluate the in vivo expression, selected ROI based on the average value over the entire FOV was taken and quantified as the mean fluorescence at different time points (20 and 30 dpi).

2.5.2. Optogenetic calibration

For each registration, ΔF/F was calculated by taking the baseline F as the mean of the signal before the optogenetic irradiation. Frames affected by skull autofluorescence induced by laser irradiation were removed. For single-pulse irradiation, 1 frame was removed; for 5-s laser irradiation, 200 frames were removed. Image resize to 256x256 was performed and 10x10 pixels ROI was selected taking account of the stimulation site. For single-pulse irradiation, peak amplitude and full width at half maximum (FWHM) were calculated. For 5-s laser irradiation, the average ΔF/F before and after irradiation was measured.

2.5.3. Whiskers stimulation

For each imaging registration, ΔF/F was calculated by taking the baseline F as the mean of the signal before the whiskers stimulation time point. Average activity maps were extrapolated from the mean of the three maximum-activity frames. Quantification of activated area was extrapolated from the binarized masks based on the threshold of Mean + 2SD. A total of 22 ROIs were then selected (11 ROI for each hemisphere, 10x10 pixels) based on the bregma coordinates and the stimulation site. Averaged sensory-evoked activity traces were extrapolated from each ROI to evaluate the differences of single area activity before and after optogenetic irradiation. Each subject underwent correlation mapping, which involved calculating the Pearson's correlation coefficient between the average signals extracted from each ROI and those of the other ROIs (during a 1-second before and after whisker stimulus (ws)), and then averaging the results within a session. Fisher's r-to-z transform was used to transform the averaged single-subject correlation maps, which were then averaged over all animals in a group. Next, the previously acquired group-related averaged maps were re-transformed to correlation values (r-scores). To display difference matrices, group differences were computed as r(AFTER)-r(BEFORE) of the averaged correlation values.

2.5.4. In vivo spike recording

For cross-talk evaluation, spike frequency was calculated in sequential 5-second time windows of LED ON/LED OFF (4 mW). For assessing the effect of 5-second laser illumination on neuronal activation, spike frequency was calculated in sequential 5-second time windows of laser ON/laser OFF (0.82 mW).

2.5.5. Ex vivo confocal imaging

The fluorescent neurons in the BFD from 4 slices were analyzed by an experienced observer to quantify the percentage of cells showing co-expression of both the indicator and the actuator.

2.6. Statistical analysis.

Paired T-Test was used for the quantification of fluorescence, in vivo spike frequency, comparison between pre- and post-irradiation activated area and peak amplitude. One-way repeated measures ANOVA followed by Bonferroni correction was performed for the quantification of single-pulse peak amplitude and FWHM. Two-way repeated measures ANOVA followed by Bonferroni correction was performed for the quantification of the average ΔF/F pre- and post-irradiation. Group-level ROI-based FC differences between before- and after-ws groups were assessed by means of one-way repeated measure ANOVA followed by Tukey correction. Errors are reported as Standard Error of Means, *$p < 0.05$, ** $p < 0.01$, *** $p < 0.001$, **** $p<0.0001$.

3. Results

In our study, we aimed to calibrate a novel all-optical system for simultaneous monitoring and inhibition of excitatory neurons. For this purpose, mice were co-injected in the retro-orbital sinus with a solution of two different PHP.eB

viruses to induce the expression of the jRCaMP1b indicator and the stGtACR2 actuator at P30. After 10 days, intact skull window surgery was performed allowing optical access to the dorsal cortex. In vivo characterization is conducted from 20 days to 40 days after the injection. Finally, ex vivo electrophysiology and confocal imaging were accomplished (Fig. 1A). Imaging sessions were also performed in a sham group of mice expressing only jRCaMP1b (Supplementary Fig. 2A).

3.1. Characterization of jRCaMP1b and stGtACR2 expression and functionality.

To evaluate the efficacy and stability of the transfection, we quantified the in vivo expression of both jRCaMP1b and stGtACR2 over time. We obtained a high level of expression of both viruses across the two imaging time points investigated (20, 30 dpi) (Fig. 1B-C). The functionality of jRCaMP1b was evaluated measuring the dorsal cortex activity across time (Fig. 1D). For stGtACR2, ex vivo electrophysiological patch-clamp recordings showed single-cell inhibition during blue-light irradiation (Fig. 1E). Using in vivo electrophysiology, we were able to verify the inhibition during the irradiation (Supplementary Fig. 1A) and the lack of stGtACR2 and jRCaMP1b cross-talk under single-photon excitation (Supplementary Fig. 1B). Histological analysis of brain slices revealed that both the indicator and actuator were largely expressed in the same neurons across the entire slice (Fig. 1F). Almost 75% of the cells expressing the jRCaMP1b indicator also expressed stGtACR2 in the BFD cortex (Fig. 1G). To sum up, we validate that a single retro-orbital injection of the mixed viruses induces stable expression and functionality of both the indicator and actuator.

3.2. All-optical calibration of optogenetic inhibition of the barrel field cortex.

The effective expression and functionality of both actuator and indicator allowed us to simultaneously manipulate and monitor neuronal activity and test the consequences of irradiation at different laser powers and durations. We first calibrated 10-ms irradiation with increased laser powers (Fig. 2A). These brief pulses on the BFD activated a neuronal response immediately after the irradiation, which is proportional in amplitude to the laser power (Fig. 2B), in line with previous findings in vivo[9][24][25]. Specifically, low laser powers (0.15 mW and 0.32 mW) did not induce any measurable activation; however, we observed the emergence of post stimulus activity in the high range (from 0.82 mW to 10.4 mW), in which there is a significant increase in the peak amplitude of the stimulated area (Fig. 2C, Supplementary table 1). Significant differences in peak duration (FWHM) are observed when comparing high laser powers with the lower range. Within the higher range, the only significant difference in the FWHM of the post stimulus response was from 0.82 mW and 6.85 mW (Fig. 2D, Supplementary table 2). Finally, we calibrated the 5-second laser irradiation for three different laser powers (0.15 mW, 0.32 mW and 0.82 mW) (Fig. 2E). We demonstrated that irradiation effectively inhibits BFD activity during the 5-s post stimulus (Fig. 2F). Within this interval, stronger inhibition was observed at the highest calibrated laser power (Fig. 2G). Importantly, this decrease of local activity is not observed in mice expressing only jRCaMP1b (Supplementary Fig. 2B-C).

3.3. Five-second laser irradiation inhibits cortical sensory-evoked response to whiskers stimulation.

We tested if our optogenetic inhibition protocol could alter the excitability of the cortex. Therefore, we investigated if optogenetic inhibition of the BFD could modulate the cortical response to whiskers stimulation. We applied the 5-s irradiation with the highest tested power (0.82 mW) on the BFD and evaluated the sensory-evoked response following the inhibition (Fig. 3A-B). We demonstrated that 5-s laser irradiation significantly decreased the size of the sensory-evoked activated area (Fig. 3C-D). Next, we compared the average sensory-evoked peak amplitude of the ipsi (right) hemisphere pre- and post-irradiation, finding a significant decrease in the sensory-evoked response (Fig. 3E). We then quantified the effects of the irradiation on the sensory-evoked activity across different cortical areas (Fig. 3F). Inhibition extends beyond the stimulated area, significantly reducing sensory-evoked peak amplitude in both the BFD and the posterior visual cortex (Vis-p) of the stimulated hemisphere (Fig. 3G). This silencing is not reported in mice expressing only jRCaMP1b (Supplementary Fig. 2D-H). Comparing the FC 1s before and after whiskers stimulation, we found a significantly reduced Pearson correlation between the stimulated BFD and the other cortical areas (Fig. 3H,I). In the irradiation condition, the FC of the stimulated BFD did not show significant differences (Fig. 3L,M). These findings highlight the local and global effects of optogenetic inhibition, demonstrating its potential for targeted modulation of cortical excitability and responsiveness to peripheral stimuli.

4. Discussion

This study presents a significant advancement in the integration of optogenetic tools and wide-field fluorescence imaging for investigating cortical dynamics. By combining the inhibitory actuator stGtACR2 with the red-shifted calcium indicator jRCaMP1b, we achieved simultaneous inhibition and monitoring of excitatory neuronal activity at the mesoscale level. Our findings reveal how localized cortical inhibition influences sensory processing and interregional connectivity, addressing critical questions about the role of cortical dynamics in behavior.

We employed a single systemic injection of a mixed solution of two PHP.eB viruses to induce the expression of jRCaMP1b and stGtACR2 in mice. This approach ensured homogeneous and stable expression over several weeks (Fig. 1), avoiding the parenchymal damage associated with invasive microinjections reported in previous studies[26][27][28]. Unlike prior optogenetic tools, which often led to unintended excitatory effects due to off-target stimulation [24][25], the specific design of stGtACR2 minimizes axonal activation while maintaining high efficacy at the soma level [9]. This specificity is crucial for interpreting the causal relationships between neuronal silencing and cortical dynamics. However, the increasing expression of stGtACR2 over the weeks (Fig. 1C) raises concerns about potential actuator toxicity. Importantly, we verified the absence of cross-talk between stGtACR2 and jRCaMP1b under single-photon excitation (Supplementary Fig. 1B), extending earlier findings with two-photon excitation using the same combination of actuator and indicator [29].

In line with other studies[30][31], 10-ms irradiation triggered a rebound of local activity, with light-dose dependent amplitude (Fig 2A-D). Either an increase in intracellular chloride or a decrease in intracellular proton concentrations could be responsible for this rebound activity. Indeed, fast variations in intracellular ion levels may cause either an efflux of chloride or an inflow of protons following light offset, which can result in rapid membrane depolarization [24][25]. In line with this hypothesis, recent studies focused on single cell inhibition through stGtACR2 reported 'paradoxical' neuron local excitation[31][32]. However, our data corroborate previous evidence [9][33] demonstrating local silencing of neuronal activity during LED irradiation both ex vivo and in vivo, respectively with patch clamp on brain slices (Fig. 1E) and LFP recordings (Supplementary Fig. 1A). Moreover, our results reveal that optogenetic inhibition using stGtACR2 leads to robust and graded suppression of spontaneous activity in the BFD up to 5s after the irradiation (Fig 2E-G).

Notably, the 5-second irradiation caused a significant reduction in both the spatial extent and amplitude of sensory-evoked responses to whisker stimulation (Fig 3B-G). This suppression extended beyond the local BFD region, involving interconnected cortical areas, including the visual cortex. Our work builds on this foundation by showing that mesoscale inhibition not only disrupts local sensory processing but also alters the network-wide coordination of cortical areas. The modulation of sensory responses by optogenetic inhibition reflects the fundamental role of distributed cortical processing in the elaboration of a sensory input [34].

These results also support the idea that connectivity patterns are crucial for explaining the paths through which inhibition flows into distant brain circuits. Indeed, local suppression subsequently alters the FC of several cortical regions. Specifically, without irradiation, whiskers stimulation induces a reduction in the FC of the stimulated BFD, indicating a weaker correlation with surrounding cortical areas (Fig. 3H,I). However, after optogenetic inhibition reduced the amplitude of the stimulus-evoked activity in the BFD, the correlation difference between pre and post stimulus becomes non-significant (Fig. 3L,M). Moreover, this disruption of FC has implications for understanding the neural basis of sensory impairments seen in disorders such as autism spectrum disorder and schizophrenia, where atypical connectivity patterns are thought to underlie perceptual deficits [35].

In conclusion, by demonstrating that the expression of both the indicator and the actuator can be achieved with a single injection, we proved the feasibility of applying this all-optical tool in animal disease models, while avoiding the complications associated with cross-breeding of multiple transgenic mouse lines.
In future studies, our tool could be leveraged to reduce the cortical sensory response in mouse models with hypersensitivity to peripheral stimuli. It would allow not only to correct behavioral anomalies associated with altered perception but also to study the immediate and long-term consequences on the cortical (dys)function. In addition, the system developed here could be adapted for brain-machine interface applications, where fine monitoring of cortical activity is essential for closed-loop control of behavior. The insights gained from our work could help optimize neural prosthetics for sensory restoration or motor rehabilitation, paving the way for more effective treatments for sensory and motor deficits.

This study establishes a novel all-optical framework for investigating the effects of targeted inhibition on mesoscale cortical dynamics. By demonstrating both local and global effects of inhibition, we provide new insights into the functional organization of cortical networks. Our findings contribute to a growing body of literature that emphasizes the importance of distributed sensory processing and highlights the potential of optogenetic tools for advancing both basic and translational neuroscience.

Disclosures

Authors declare no competing interests.

Code, Data, and Materials Availability

The data that support the findings of this study are available on request from the corresponding author.

Acknowledgements

This work has been funded by Telethon Seed Grant Spring 2022 PHEM (GSA22E006), the Italian Ministry of Universities and Research PRIN 2022 (2022YCTLPL), project THE Tuscany Health Ecosystem (ECS_00000017), MUR_ PNRR, Banca di Italia and Fondo di Beneficenza di Intesa Sanpaolo RICONSIN project (B/2021/0202), Ricerca Scientifica e Tecnologica della Fondazione Cassa di Risparmio di Firenze (CRF2020). In addition, this project has been supported by the framework of Eurobioimaging (ESFRI research infrastructure) - Advanced Light Microscopy Italian Node. Figures 1A,E, 2A, 2E, 3A and Supplementary Figure 2A were created using BioRender.

Contribution

ALAM conceived the study.

ALAM, MA and EM designed and interpreted experiments and computational analyses.

MA, EM, LC and FR performed experiments and generated data.

MA, EM and FR conducted computational analyses.

MA, EM and ALAM drafted the manuscript.

LC, FR edited the manuscript.

ALAM, FSP, AM, GM contributed funding and resources.

All authors participated in the review of the manuscript.

References

[1] J. Deubner, P. Coulon, and I. Diester, "Optogenetic approaches to study the mammalian brain," Aug. 01, 2019, *Elsevier Ltd*. doi: 10.1016/j.sbi.2019.04.003.

[2] A. R. Acharya *et al.*, "In vivo blue light illumination for optogenetic inhibition: Effect on local temperature and excitability of the rat hippocampus," *J Neural Eng*, vol. 18, no. 6, Dec. 2021, doi: 10.1088/1741-2552/ac3ef4.

[3] K. Deisseroth, "Optogenetics," Jan. 2011. doi: 10.1038/nmeth.f.324.

[4] P. S. A. Kalanithi and J. M. Henderson, "Optogenetic Neuromodulation," in *International Review of Neurobiology*, vol. 107, Academic Press Inc., 2012, pp. 185–205. doi: 10.1016/B978-0-12-404706-8.00010-3.

[5] C. Gasselin, B. Hohl, A. Vernet, S. Crochet, and C. C. H. Petersen, "Cell-type-specific nicotinic input disinhibits mouse barrel cortex during active sensing," *Neuron*, vol. 109, no. 5, pp. 778-787.e3, Mar. 2021, doi: 10.1016/j.neuron.2020.12.018.

[6] E. G. Govorunova, O. A. Sineshchekov, R. Janz, X. Liu, and J. L. Spudich, "Natural light-gated anion channels: A family of microbial rhodopsins for advanced optogenetics," *Science (1979)*, 2015, doi: DOI:10.1126/science.aaa7484.

[7] J. E. Messier, H. Chen, Z.-L. Cai, and M. Xue, "Targeting light-gated chloride channels to neuronal somatodendritic domain reduces their excitatory effect in the axon," *Elife*, 2018, doi: 10.7554/eLife.38506.001.

[8] J. Park, J. W. Phillips, J.-Z. Guo, K. A. Martin, A. W. Hantman, and J. T. Dudman, "Motor cortical output for skilled forelimb movement is selectively distributed across projection neuron classes," 2022. doi: 10.1126/sciadv.abj5167.

[9] M. Mahn *et al.*, "High-efficiency optogenetic silencing with soma-targeted anion-conducting channelrhodopsins," *Nat Commun*, vol. 9, no. 1, Dec. 2018, doi: 10.1038/s41467-018-06511-8.

[10] V. Emiliani, A. E. Cohen, K. Deisseroth, and M. Häusser, "All-optical interrogation of neural circuits," Oct. 14, 2015, *Society for Neuroscience*. doi: 10.1523/JNEUROSCI.2916-15.2015.

[11] J. Akerboom *et al.*, "Genetically encoded calcium indicators for multi-color neural activity imaging and combination with optogenetics," *Front Mol Neurosci*, no. FEB, Feb. 2013, doi: 10.3389/fnmol.2013.00002.

[12] A. Scaglione, F. Resta, F. Goretti, and F. S. Pavone, "Group ICA of wide-field calcium imaging data reveals the retrosplenial cortex as a major contributor to cortical activity during anesthesia," *Front Cell Neurosci*, vol. 18, 2024, doi: 10.3389/fncel.2024.1258793.

[13] E. Montagni *et al.*, "Wide-field imaging of cortical neuronal activity with red-shifted functional indicators during motor task execution," *J Phys D Appl Phys*, vol. 52, no. 7, Feb. 2019, doi: 10.1088/1361-6463/aaf26c.

[14] V. Esmaeili *et al.*, "Rapid suppression and sustained activation of distinct cortical regions for a delayed sensory-triggered motor response," *Neuron*, vol. 109, no. 13, pp. 2183-2201.e9, Jul. 2021, doi: 10.1016/j.neuron.2021.05.005.

[15] M. Kondo and M. Matsuzaki, "Neuronal representations of reward-predicting cues and outcome history with movement in the frontal cortex," *Cell Rep*, vol. 34, no. 5, Feb. 2021, doi: 10.1016/j.celrep.2021.108704.

[16] S. Yamada, Y. Wang, and H. Monai, "Transcranial cortex-wide Ca2+ imaging for the functional mapping of cortical dynamics," 2023, *Frontiers Media S.A.* doi: 10.3389/fnins.2023.1119793.

[17] D. H. Lim, M. H. Mohajerani, J. Ledue, J. Boyd, S. Chen, and T. H. Murphy, "In vivo large-scale cortical mapping using channelrhodopsin-2 stimulation in transgenic mice reveals asymmetric and reciprocal relationships between cortical areas," *Front Neural Circuits*, no. FEBRUARY, Feb. 2012, doi: 10.3389/fncir.2012.00011.

[18] T. C. Harrison, O. G. S. Ayling, and T. H. Murphy, "Distinct Cortical Circuit Mechanisms for Complex Forelimb Movement and Motor Map Topography," *Neuron*, vol. 74, no. 2, pp. 397–409, Apr. 2012, doi: 10.1016/j.neuron.2012.02.028.

[19] E. Conti, A. L. A. Mascaro, and F. S. Pavone, "Large scale double-path illumination system with split field of view for the all-optical study of inter-and intra-hemispheric functional connectivity on mice," 2019, *MDPI AG*. doi: 10.3390/mps2010011.

[20] E. Conti *et al.*, "Combining Optogenetic Stimulation and Motor Training Improves Functional Recovery and Perilesional Cortical Activity," *Neurorehabil Neural Repair*, vol. 36, no. 2, pp. 107–118, Feb. 2022, doi: 10.1177/15459683211056656.

[21] F. Resta, E. Montagni, G. de Vito, A. Scaglione, A. L. Allegra Mascaro, and F. S. Pavone, "Large-scale all-optical dissection of motor cortex connectivity shows a segregated organization of mouse forelimb representations," *Cell Rep*, vol. 41, no. 6, Nov. 2022, doi: 10.1016/j.celrep.2022.111627.

[22] L. Z. Fan *et al.*, "All-Optical Electrophysiology Reveals the Role of Lateral Inhibition in Sensory Processing in Cortical Layer 1," *Cell*, vol. 180, no. 3, pp. 521-535.e18, Feb. 2020, doi: 10.1016/j.cell.2020.01.001.

[23] E. Montagni *et al.*, "Age-dependent cortical overconnectivity revers under anesthesia in Shank3 mice," Aug. 16, 2024. doi: 10.1101/2024.08.13.607775.

[24] J. S. Wiegert, M. Mahn, M. Prigge, Y. Printz, and O. Yizhar, “Silencing Neurons: Tools, Applications, and Experimental Constraints,” Aug. 02, 2017, *Cell Press*. doi: 10.1016/j.neuron.2017.06.050.

[25] M. Mahn, M. Prigge, S. Ron, R. Levy, and O. Yizhar, “Biophysical constraints of optogenetic inhibition at presynaptic terminals,” *Nat Neurosci*, vol. 19, no. 4, pp. 554–556, Mar. 2016, doi: 10.1038/nn.4266.

[26] A. S. Hamodi, A. M. Sabino, N. D. Fitzgerald, D. Moschou, and M. C. Crair, “Transverse sinus injections drive robust whole-brain expression of transgenes,” *Elife*, vol. 9, pp. 1–16, May 2020, doi: 10.7554/eLife.53639.

[27] S. Lohani *et al.*, “Spatiotemporally heterogeneous coordination of cholinergic and neocortical activity,” *Nat Neurosci*, vol. 25, no. 12, pp. 1706–1713, Dec. 2022, doi: 10.1038/s41593-022-01202-6.

[28] L. V. Vinogradova, M. P. Rysakova, and I. V. Pavlova, “Small damage of brain parenchyma reliably triggers spreading depolarization,” *Neurol Res*, vol. 42, no. 1, pp. 76–82, Jan. 2020, doi: 10.1080/01616412.2019.1709745.

[29] A. Forli *et al.*, “Two-Photon Bidirectional Control and Imaging of Neuronal Excitability with High Spatial Resolution In Vivo,” *Cell Rep*, vol. 22, no. 11, pp. 3087–3098, Mar. 2018, doi: 10.1016/j.celrep.2018.02.063.

[30] N. Li *et al.*, “Spatiotemporal constraints on optogenetic inactivation in cortical circuits,” *Elife*, vol. 8, Nov. 2019, doi: 10.7554/eLife.48622.

[31] N. R. Kinsky *et al.*, “Simultaneous electrophysiology and optogenetic perturbation of the same neurons in chronically implanted animals using µLED silicon probes,” *STAR Protoc*, vol. 4, no. 4, Dec. 2023, doi: 10.1016/j.xpro.2023.102570.

[32] L. Watkins de Jong, M. M. Nejad, E. Yoon, S. Cheng, and K. Diba, “Optogenetics reveals paradoxical network stabilizations in hippocampal CA1 and CA3,” *Current Biology*, vol. 33, no. 9, pp. 1689-1703.e5, May 2023, doi: 10.1016/j.cub.2023.03.032.

[33] Y. Murata and M. T. Colonnese, “GABAergic interneurons excite neonatal hippocampus in vivo,” *Science Advance*, 2020, doi: 10.1126/sciadv.aba1430.

[34] I. Ferezou, F. Haiss, L. J. Gentet, R. Aronoff, B. Weber, and C. C. H. Petersen, “Spatiotemporal Dynamics of Cortical Sensorimotor Integration in Behaving Mice,” *Neuron*, vol. 56, no. 5, pp. 907–923, Dec. 2007, doi: 10.1016/j.neuron.2007.10.007.

[35] L. Balasco *et al.*, “Abnormal whisker-dependent behaviors and altered cortico-hippocampal connectivity in Shank3b-/-mice,” *Cerebral Cortex*, vol. 32, no. 14, pp. 3042–3056, Jul. 2022, doi: 10.1093/cercor/bhab399.

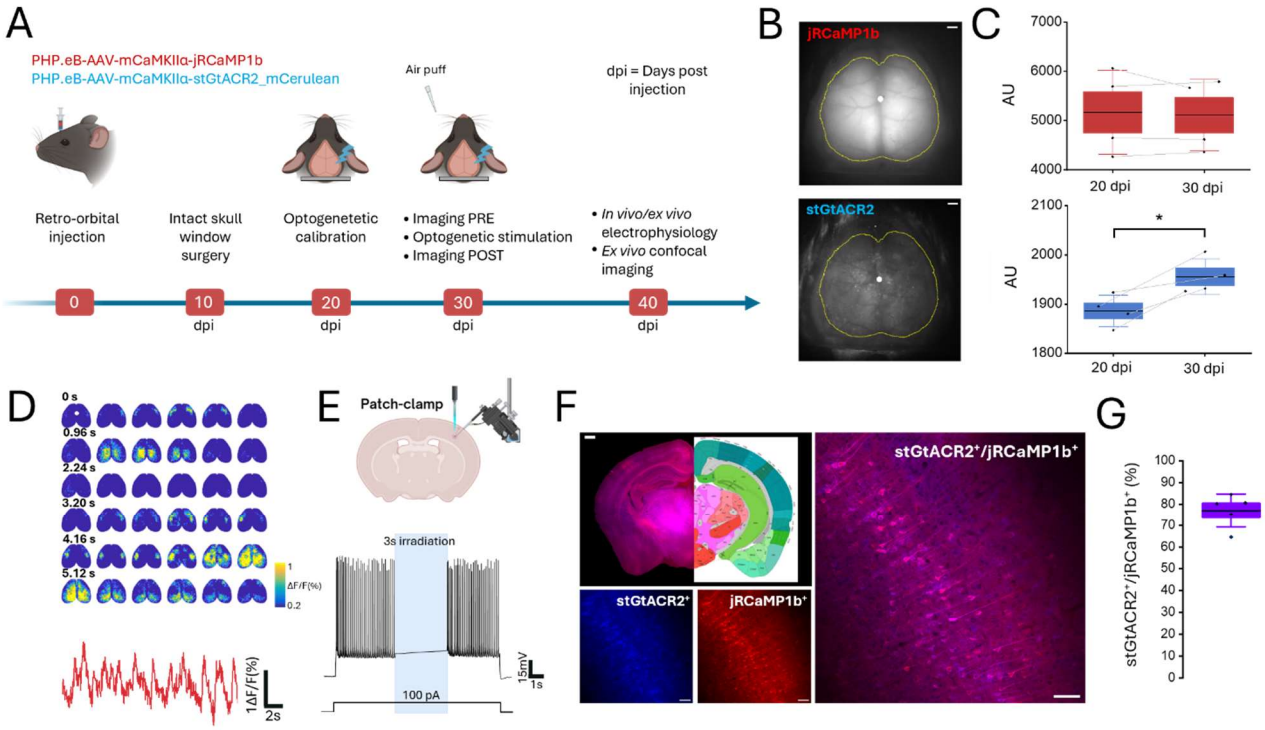

Figure 1. Experimental timeline and characterization of jRCaMP1b-stGtACR2 expression and functionality. (A) Experimental timeline with retro-orbital injection of both jRCaMP1b and stGtACR2, optical window surgery 10 days post injection (dpi), in vivo imaging sessions 20 and 30 dpi and in vivo electrophysiology 40 dpi. After in vivo experiments, ex vivo electrophysiology and confocal imaging analysis were performed. **(B)** Representative images of the field of view of jRCaMP1b (red) and stGtACR2 (blue). Yellow lines represent the selected ROI for analysis. White dot represents bregma, scale bar: 1mm. **(C)** in vivo quantification of jRCaMP1b (red) and stGtACR2 (blue) expression (red 20dpi: 5168±423 arbitrari unit (AU); red 30dpi:5111±362 AU; blue 20dpi: 1886±16 AU; blue 30dpi:1955±18 AU; n=4; *p=0.02 Paired Sample t Test). **(D)** Top: Representative image sequence of jRCaMP1b resting state cortical activity. White dot represents bregma, scale bar: 1mm. Bottom: Representative trace of jRCaMP1b activity. **(E)** Top: Representative image of ex vivo electrophysiology paradigm. Bottom: Representative trace of neuronal activity before, during and after 3s optogenetic irradiation (blue). **(F)** Upper left: Representative wide-field image of a single slice with related Allen Brain Atlas reference, scale bar: 1mm. Bottom left: Representative confocal images showing the neuronal expression of jRCaMP1b (red) and stGtACR2 (blue) in the barrel field cortex, scale bar: 100 µm. Right: Merge of the representative images, scale bar: 100 µm. **(G)** Quantification of the colocalization ratio stGtACR2^{+}/ jRCaMP1b^{+} (73±3 %, n=4 slices, 1 mouse).

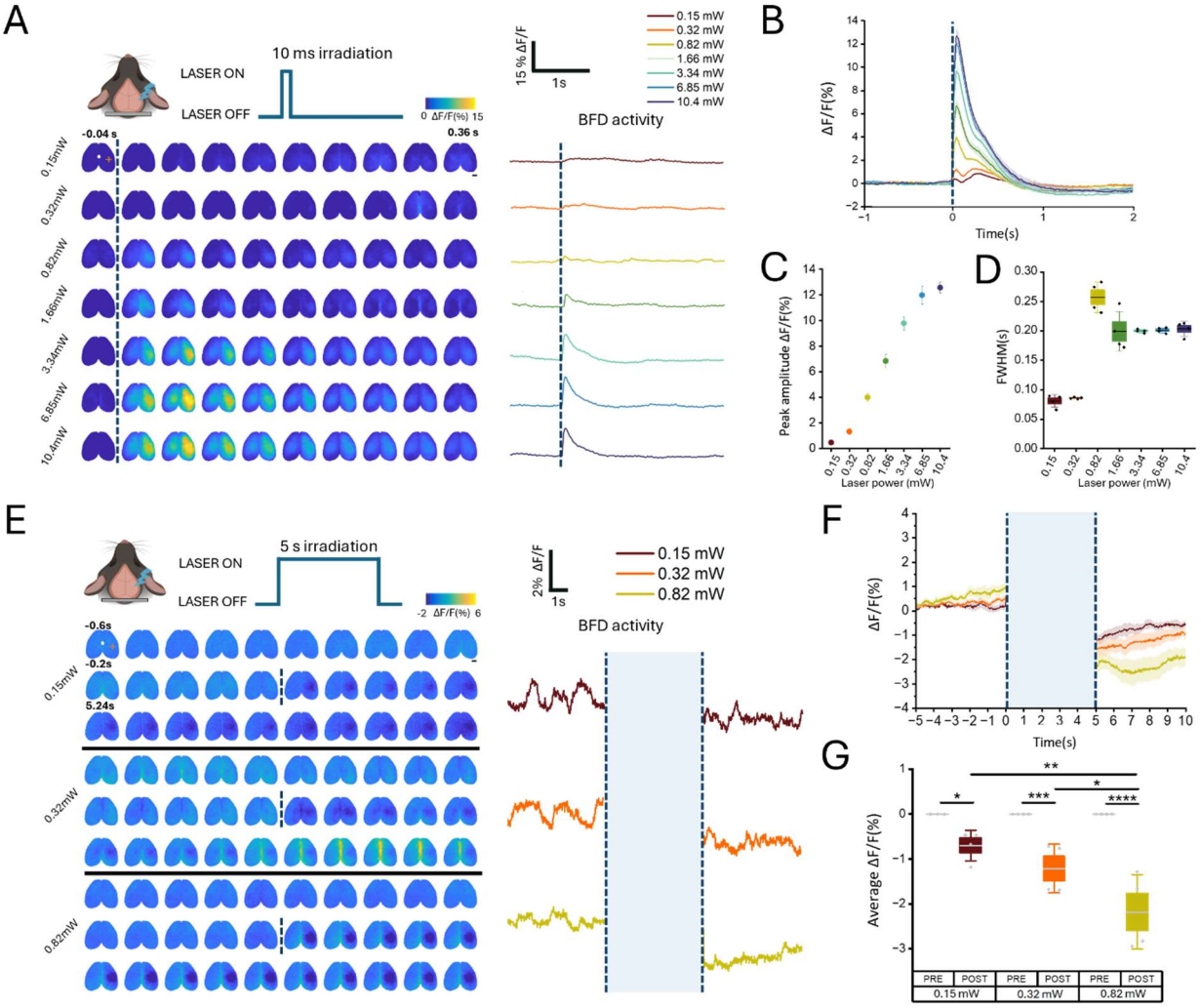

Figure 2. Optogenetic calibration of stGtACR2 stimulation at different laser power. (A) Left: Representative image sequence of cortical activity before and after 10-ms blue-light irradiation on the barrel-field (BFD) at increasing laser power. Frame with optogenetic back-scattering is removed. Dashed line represents the stimulation time point. White dot represents bregma. Orange cross represents the stimulated site. Scalebar: 2mm. Right: Representative traces of BFD activity at increasing laser power. Dashed line represents the stimulation time point. **(B)** BFD activity before and after 10-ms blue-light irradiation (dashed line) at increasing laser power. **(C-D)** Quantification of peak amplitude (C) and FWHM (D) at increasing laser power (peak amplitude: 0.15mW: 1.2±0.14%; 0.32mW: 1.6±0.13%; 0.82mW: 4.6±0.29%; 1.66mW: 7.3±0.44%; 3.34mW: 10.3±0.45%; 6.85mW: 12.3±0.68%; 10.4mW: 13.11±0.32%. FWHM: 0.15mW: 0.081±0.005s; 0.32mW: 0.0852±0.0007s; 0.82mW: 0.25±0.01s; 1.66mW: 0.198±0.017s; 3.34mW: 0.199±0.001s; 6.85mW: 0.201±0.002s; 10.4mW: 0.203±0.006s. n-mice=4, n-stim=10. See supplementary table 1,2 for significance). **(E)** Left: Representative image sequence of cortical activity before and after 5-s blue-light irradiation on the BFD at increasing laser power. Frames with optogenetic back-scattering are removed. Dashed line represents the removed stimulation interval. White dot represents bregma. Orange cross represents the stimulated site. Scalebar: 2mm. Right: Representative traces of BFD activity at increasing laser power. Dashed lines represent the stimulation interval. **(F-G)** Averaged BFD activity before and after 5-s blue-light irradiation at different laser power (F) with relative quantification of average ΔF/F (G). Dashed lines represent the stimulation interval (0.15mW PRE: $0.001 \pm 5.9 * 10^{-4}$ %; POST: -0.69±0.17%; 0.32mW PRE: $7.8 * 10^{-4} \pm 1.5 * 10^{-4}$ %; POST: -1.21±0,27%; 0.82mW PRE: $0.001 \pm 5.6 * 10^{-4}$ %; POST: -2.17±0.41%; n-mice=4, n-stim=10).

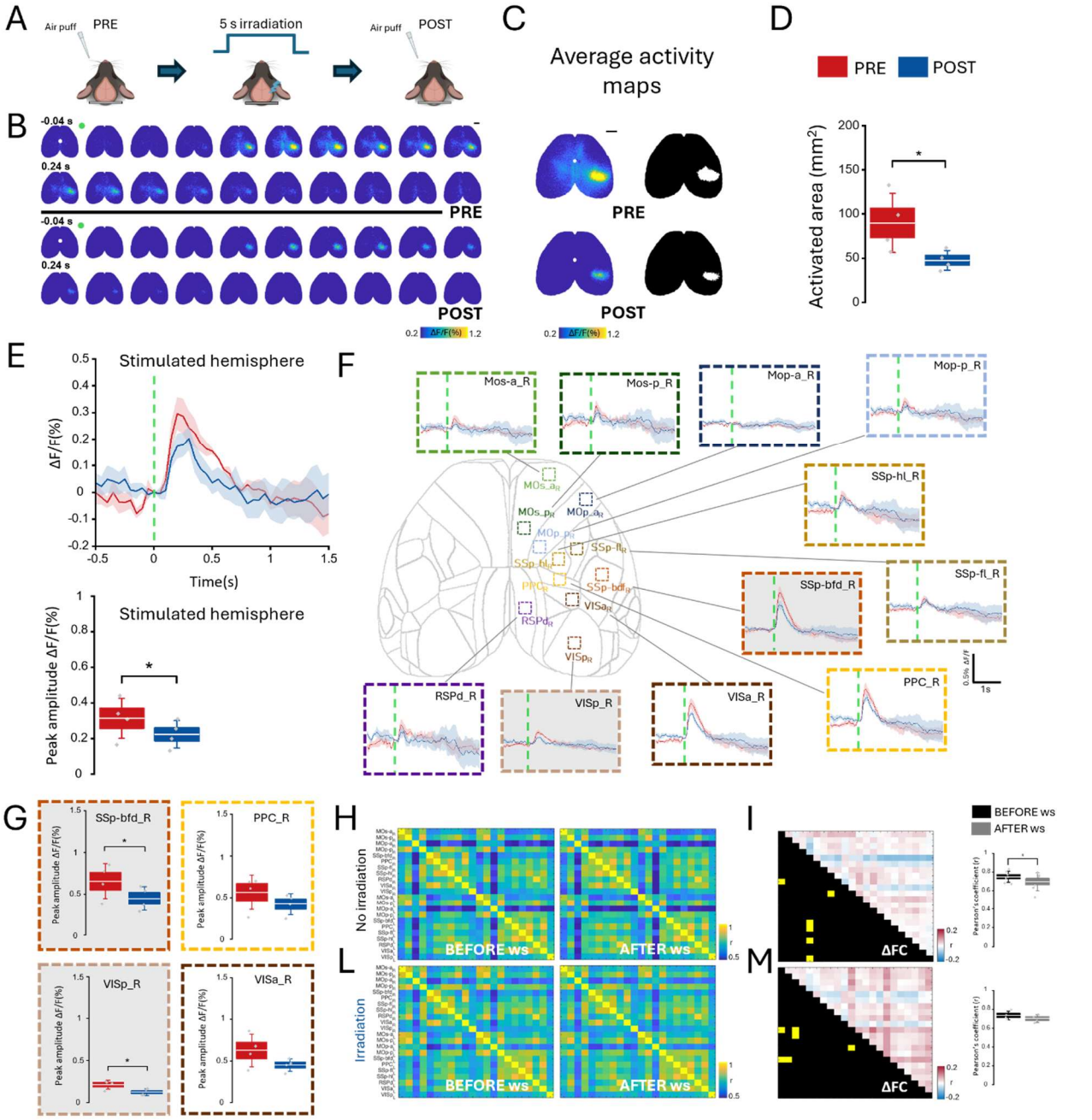

Figure 3. Effects of 5-second optogenetic stimulation on cortical sensory-evoked response. (A) Experimental setup with whisker stimulation before (left) and after (right) 5-s laser irradiation (middle). **(B)** Representative activation sequence of sensory-evoked response to whiskers stimulation before and after 5-s laser irradiation. Green dot represents the whisker stimulus time point. White dot represents bregma, scale bar: 2mm. **(C)** Left: Representative image of average activity maps before (pre) and after (post) 5-s laser irradiation with the correspondent binarized mask (right). White dot represents bregma, scale bar: 2mm. **(D)** Quantification of activated area before (red) and after (blue) optogenetic irradiation (PRE: 89.8±16.7 mm^2; POST: 47.57±5.59 mm^2; N=4; *p=0.03, Paired Sample t Test). **(E)** Sensory-evoked activity of the right (ipsi) hemisphere before (red) and after (blue) 5-s optogenetic irradiation (top) with the correspondent quantification (bottom) (ipsi PRE: 0.31±0.05%; ipsi POST: 0.22±0.03%; n mice=4, n stim=40; *p=0.02, Paired Sample t Test). Dashed line indicates the whiskers stimulation time point. **(F-G)** Cortical parcellation with the relative sensory-evoked activity (G) before (red) and after (blue) optogenetic inhibition; quantification of representative areas peak amplitude (H) (Ssp-bfd_R PRE: 0.6±0.1%; Ssp-bfd_R POST: 0.44±0.07%; *p=0.01; PPC_R PRE: 0.5±0.1%; PPC_R POST: 0.42±0.06%; p=0.07; VISp_R PRE: 0.21±0.02%; VISp_R POST: 0.12±0.01%; *p=0.02; VISa_R PRE: 0.62±0.09%; VISa_R POST: 0.44±0.03%; p=0.06; n mice=4, n stim=40). Dashed lines indicate the whiskers stimulation time point. Grey wallpaper indicates only significant areas. **(H)** No-irradiation condition: Pairwise Pearson's correlation coefficients visualized as average matrices of baseline- (left) and evoked-activity (right). **(I)** No-irradiation condition: (Left) Difference matrix of functional connectivity (FC) pre- and post-whisker stimulation (ws). Red and blue indicate POST hyper- or hypo-connectivity, with significant differences in yellow (*p<0.05; N=7, 40 stimulations). (Right) BFD connectivity quantification pre- (black)

447 **Figure 3 Continued** and post-ws (grey): PRE: 0.74±0.02r; POST: 0.69±0.03r; *p=0.048, Paired Sample t Test). **(L)** Irradiation condition: Pairwise
448 Pearson's correlation coefficients visualized as averaged matrices of baseline- (left) and evoked-activity (right). **(M)** Irradiation condition: (Left)
449 Difference matrix of FC pre- and post-ws. Red and blue indicate POST hyper- or hypo-connectivity, with significant differences in yellow (*p<0.05;
450 N=4, 40 stimulations). (Right) BFD connectivity quantification pre- (black) and post-ws (grey): PRE: 0.73±0.02r; POST: 0.70±0.02r).

451

452

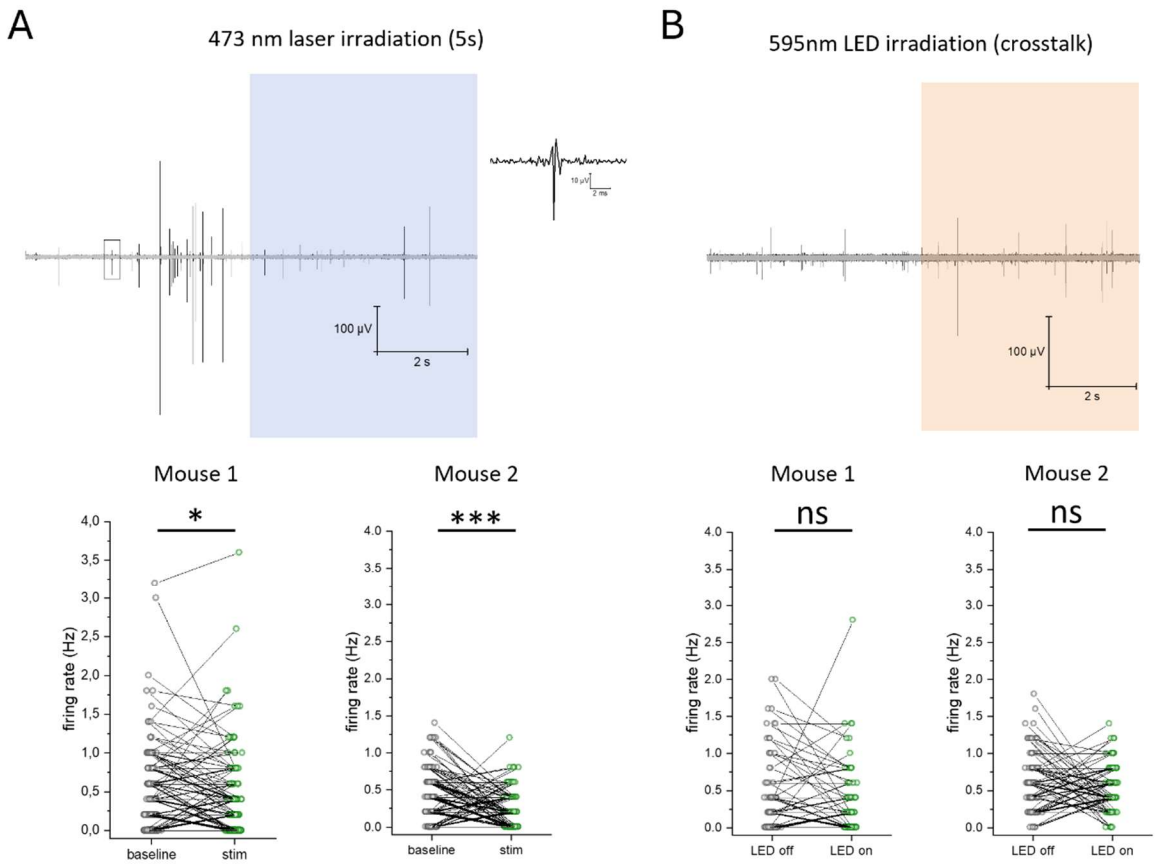

Supplementary Fig. 1 Electrophysiological validation of optogenetic inhibition and stimulation/imaging crosstalk. (A) *Top*: Representative traces showing spikes. The 5-second optogenetic stimulation period is represented by the light blue square. *Inset*: Magnified view of the highlighted spike. *Bottom*: Quantification of the firing rate in two mice. Both mice show a significant reduction in the firing rate during the optogenetic inhibition period. **(B)** *Top*: Representative traces showing spikes. The LED-ON period is represented by the light orange square. *Bottom*: Quantification of the firing rate in two mice. Both show no significant alteration in firing rate during the illumination used for imaging sessions.

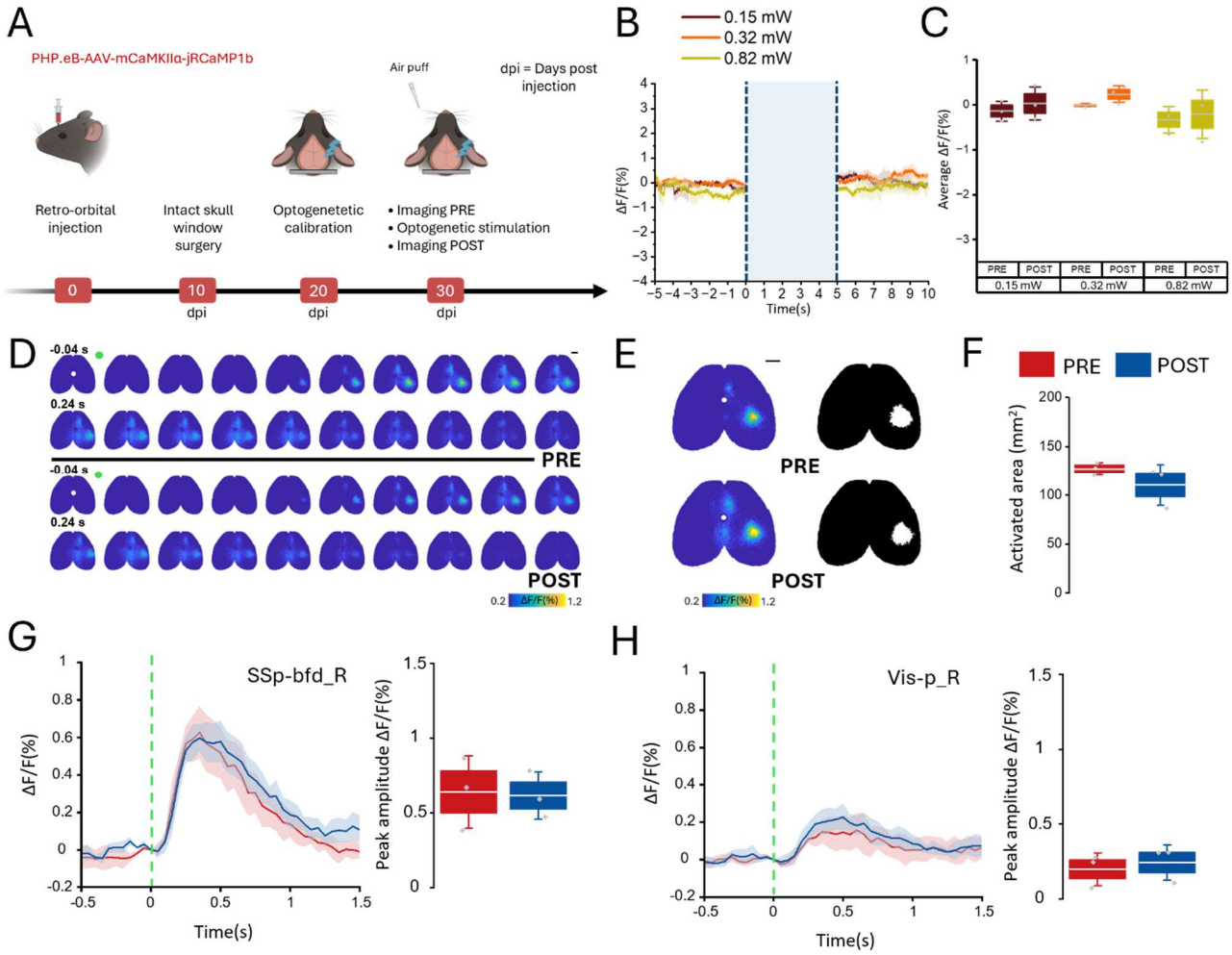

Supplementary Fig. 2 Effects of 5-s laser irradiation on mice not expressing stGtACR2. (A) Experimental timeline with retro-orbital injection of jRCaMP1b, optical window surgery 10 days after injection(dpi) and in vivo imaging session 20 dpi. **(B-C)** Averaged BFD activity before and after 5-s of optogenetic stimulation at different laser power (B) with relative quantification of average ΔF/F (C). Dashed lines represent the stimulation interval (0.15mW PRE: -0.13±0.12 %; POST: 0.03±0.21%; 0.32mW PRE: -0.007±0.02 %; POST: 0.2±0.1%; 0.82mW PRE: -0.32±0.16%; POST: -0.2±0.3%; n-mice=3, n-stim=10). **(D)** Representative activation sequence of sensory-evoked response to whiskers stimulation before and after 5-s laser irradiation. Green dot represents the whisker stimulus time point. White dot represents bregma, scale bar: 2mm. **(E)** Representative image of average activity maps before (*left*) and after (*right*) 5-s laser irradiation (*top*) with relative binarized masks (*bottom*). White dot represents bregma, scale bar: 2mm. **(F)** *:* Quantification of activated area before (red) and after (blue) optogenetic irradiation (PRE: 127.2±3.7 mm^2; POST: 110.4±12.0 mm^2; nmice=3). **(G)** Sensory-evoked activity of the BFD cortex before (red) and after (blue) optogenetic irradiation and quantification of peak amplitude (PRE: 0.63±0.13%; POST: 0.61±0.09%; nmice=3, nstim=40). **(H)** Sensory-evoked activity of the Visual cortex before (red) and after (blue) optogenetic irradiation and quantification of peak amplitude (PRE: 0.19±0.06%; POST: 0.24±0.07%; nmice=3, nstim=40).

Powers	t Value	Prob>t	Sign.
0.15-0.32 mW	1.05648	1	ns
0.15-0.82 mW	9.44133	4.50896E-7	****
0.15-1.66mW	17.00494	3.26088E-11	****
0.15-3.34mW	25.63564	2.6817E-14	****
0.15-6.85mW	31.23952	8.23003E-16	****
0.15-10.4mW	33.2844	2.67772E-16	****
0.32-0.82mW	8.38485	2.61899E-6	****
0.32-1.66mW	15.94846	9.66218E-11	****
0.32-3.34mW	24.57916	5.60679E-14	****
0.32-6.85mW	30.18304	1.51202E-15	****
0.32-10.4mW	32.22792	4.74201E-16	****
0.82-1.66mW	7.5636	1.13334E-5	****
0.82-3.34mW	16.19431	7.46266E-11	****
0.82-6.85mW	21.79819	4.55306E-13	****
0.82-10.4mW	23.84307	9.54272E-14	****
1.66-3.34mW	8.6307	1.71799E-6	****
1.66-6.85mW	14.23458	6.48118E-10	****
1.66-10.4mW	16.27946	6.82943E-11	****
3.34-6.85mW	5.60388	5.38007E-4	***
3.34-10.4mW	7.64876	9.6961E-6	****
6.85-10.4mW	2.04488	1	ns

Supplementary Table 1. One-way repeated measures ANOVA for quantification of peak amplitude in single-pulse irradiation. Comparison between coupled powers with relative t Value, Prob>t and significance. *p < 0.05, ** p < 0.01, *** p < 0.001, **** p<0.0001.

Powers	t Value	Prob>t	Sign.
0.15-0.32 mW	2.44854	0.52118	ns
0.15-0.82 mW	2.83438	0.23089	ns
0.15-1.66mW	5.88381	3.0051E-4	***
0.15-3.34mW	6.01137	2.31225E-4	***
0.15-6.85mW	6.39831	1.05774E-4	***
0.15-10.4mW	6.24374	1.44221E-4	***
0.32-0.82mW	5.28292	0.00106	**
0.32-1.66mW	8.33236	2.86858E-6	****
0.32-3.34mW	8.45991	2.30081E-6	****
0.32-6.85mW	8.84685	1.19326E-6	****
0.32-10.4mW	8.69228	1.54764E-6	****
0.82-1.66mW	3.04943	0.14492	ns
0.82-3.34mW	3.17699	0.10962	ns
0.82-6.85mW	3.56393	0.04658	*
0.82-10.4mW	3.40936	0.06565	ns
1.66-3.34mW	0.12755	1	ns
1.66-6.85mW	0.5145	1	ns
1.66-10.4mW	0.35993	1	ns
3.34-6.85mW	0.38694	1	ns
3.34-10.4mW	0.23237	1	ns
6.85-10.4mW	0.15457	1	ns

Supplementary Table 2. One-way repeated measures ANOVA for quantification of FWHM in single-pulse irradiation.
Comparison between coupled powers with relative t Value, Prob>t and significance. *$p < 0.05$, ** $p < 0.01$, *** $p < 0.001$, **** $p<0.0001$.